Stress Corrosion Cracking and Anodic Dissolution Behavior of 5083 Aluminum Alloy†

Tadashi TAKEMOTO* and Ikuo OKAMOTO**

Abstract

The effect of applied tensile stress and continuous strain on the dissolution behavior of 5083 aluminum alloy has been investigated in relation to the stress corrosion cracking susceptibility of short transverse direction of the alloy. Stress corrosion cracking tests were carried out by means of constant strain rate tequniques under various anodic potentials. Aqueous solution of 1.0 mol/ℓ NaCl + 0.1 mol/ℓ H_2O_2 ajusted at pH 11.0 was used as corrosive solution. Strained electrode reactions were also studied as functions of tensile stress, continuous strain, electrode potential and microstructure. The potential that the anodic current in polarization curves began to increase from the constant current density similar to passive state was defined as the breakdown potential (E_b). E_b was found to depend on polarization rate, the amount of grain boundary precipitate and applied tensile stress. The potential that does not provide stress corrosion cracking could be expressed by using both the potentials that does not labilized the surface oxide film after holding at the potential for certain times and the stress dependence of E_b.

KEY WORDS: (Stress Corrosion) (Al-Mg Alloys) (Cracking) (Strain) (Corrosion Tests) (Halides)

1. Introduction

Many studies have been performed on the stress corrosion cracking (SCC) of 5083 aluminum alloy in relations to both structural factors of materials and environmental factors; and the cracking mechanism is becoming relatively clear. Especially, since the cracking path of Al-Mg alloys proceeds intergranularly, the relations between grain boundary precipitates (β-phase, Mg_2Al_3) and the susceptibility have been studied[1), 2)]. The grain boundary phases preferentially dissolves easily due to its less noble electrode potential than grain interior[3), 4)], and excert an marked influence on the grain boundary corrosion[5)] and SCC[6)-9)]. Therefore, good correlations existed between the precipitation amount at grain boundary (the area ratio of occupied grain boundary precipitates to total grain boundary) and the SCC life[10), 11)]. The electrochemical dissolution at grain boundaries seems to be an important factor of SCC because the susceptibility to grain boundary corrosion coincides well with that of SCC[5), 12)], however, the relations between the microstructural change and SCC susceptibility of the alloy are not explained sufficiently by only the potential difference between grain interior and grain boundary precipitates[13)]. Therefore, it is important to discuss the SCC behavior by considering the effect of stress or strain on grain boundary corrosion and anodic dissolution reactions.

In recent times, the role of surface films in anodic dissolution reaction[14)] and the break down potential of grain boundary and grain interior have been investigated by the use of strain electrode techniques, and the SCC propagation mechanisms were discussed[15)]. The SCC cracks of Al-Mg alloys have been known to proceed along grain boundaries. From the stand point of mechano-chemical mechanism, preferential dissolution mechanism at grain boundary under stress, the effect of applied stress and strain on the break down of surface films and anodic dissolution behaviour have not been clarified sufficiently yet. The aim of the present work is to clarify the point using constant strain rate tensile test under anodic potentials. Anodic polarization behavior under applied tensile load and fracture surface observations were also conducted.

2. Experimental Procedures

The chemical composition of the 5083-O alloy is as follows; Mg : 4.60, Mn : 0.69, Fe : 0.18, Si : 0.14, Cr : 0.12, Cu : 0.01, Ti : 0.01, Al : bal., (wt%). To investigate the SCC susceptibility of short transverse direction (ST

† Received on November 1, 1984.
* Research Instructor
** Professor

Transactions of JWRI is published by Welding Research Institute of Osaka University, Ibaraki, Osaka 567, Japan

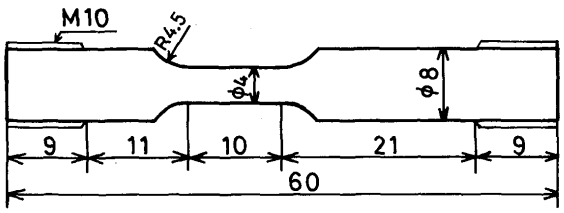

Fig. 1 Shape and size of SCC test specimen

direction) of 5083 aluminum alloy of 61 mm thickness, SCC test specimens were machined in order that the tensile direction is parallel to the ST direction as indicated in **Fig. 1**. The heat treatment of the specimens are following three types: solution treated (450°C, 24 hr), aged (aged at 150°C for 168 hr after solution treatment at 450°C for 24 hr), and as received. In aged materials, the almost continuous existence of β-phase at grain boundaries is confirmed by the transmission electron microscopic observation.

SCC tests were carried out under constant applied strain rate and anodic polarization by the use of an Instron type tensile test machine and a potentiostat. Prior to SCC test emery-polished specimens were electropolished in perchloric acid-ethyl alcohol bath, and then rinsed sufficiently in tap water. The composition of SCC test solution is 1.0 mol/ℓ NaCl + 0.1 mol/ℓ H_2O_2, which is adjused at pH 11.0 by the addition of 10% NaOH. The alkaline solution makes the initiation potential of active dissolution clear[15]. A specimen was attached to an Instron type tensile test machine through insulation jigs. After immersion in the test solution (500 mℓ), the potential of specimen was fixed at −1250 mV (vs. saturated calomel electrode, SCE) by a potentiostat and then moved toward noble direction by a step scanning equipment (scanning rate: 20 mV/min) up to the predetermined anodic potential. SCC tests were conducted under constant strain rate of 8.33×10^{-5}/sec (cross head speed: 0.05 mm/min). Elongation to fracture, ultimate tensile strength (UTS), and anodic current were measured to evaluate the SCC susceptibility as functions of applied anodic potentials and heat treatment of the alloy. Fractured specimens were immeadiately removed from the test solution and rinsed in ethyl alcohol.

Scanning electron microscopic observation, energy dispersive X-ray analysis and polarization measurements on flat plate with ST surface under no applied load were also conducted.

3. Experimental Results

3.1 Anodic polarization behavior

Figure 2 shows the effect of step sweep rates on anodic polarization curves. The natural electrode potential of the alloy was about −1300 mV, step sweep rate of 20 mV/

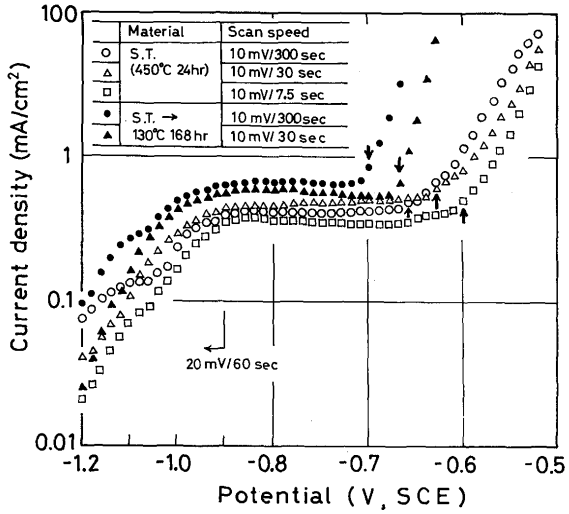

Fig. 2 Anodic polarization curves of 5083 aluminum alloy under various step sweep rates

min was adopted from the natural electrode poptential to −900 mV. Above −900 mV sweep rate changed as shown in Fig. 2. Between −900 ~ −700 mV, the curves showed constant current density similar to passivated region, however, above certain potentials indicated by arrows, anodic current increased immeadiately with the increase of applied potentials. The drastic increament is corresponded that the potential exceeded the so called activation potential[16], as a result, the surface film is shifted from stable to unstable state. In this paper, the potential is designated as the surface film breakdown potential (E_b)*. E_b is found to depend on step sweep rate (polarization rate), microstructure of specimen and applied stress. The effect of step sweep rate is shown in Fig. 2; E_b shifted toward base direction as the step sweep rate became slow. In aged specimens, β-phase is continuously precipitated along grain boundaries, E_b is about 40 mV lower than solution treated ones.

Fig. 3 indicates the effect of applied tensile stress on E_b. Since the difference of E_b which is caused by the difference of heat treatment can be obtained irrespective to the polarization rate (Fig. 2), the polarization rate of 10 mV/sec was used. Applied tensile stress shifted E_b toward base direction and the surface film became unstable at lower potentials with the increase of applied stress. Since E_b of aged specimens are always lower than that of solution treated ones under all applied stresses, the reason of the decrease of E_b with the increase of applied stress is attributed to the break down of the surface films at grain boundary and/or precipitate/matrix interface by the stress

* E_b corresponds the so called pitting potential, however, the potential is dependent not only on the microstructure of specimen but also on the experimental conditions such as polarization rate and applied stress. Consequently, the above mentioned designation is adopted in this article.

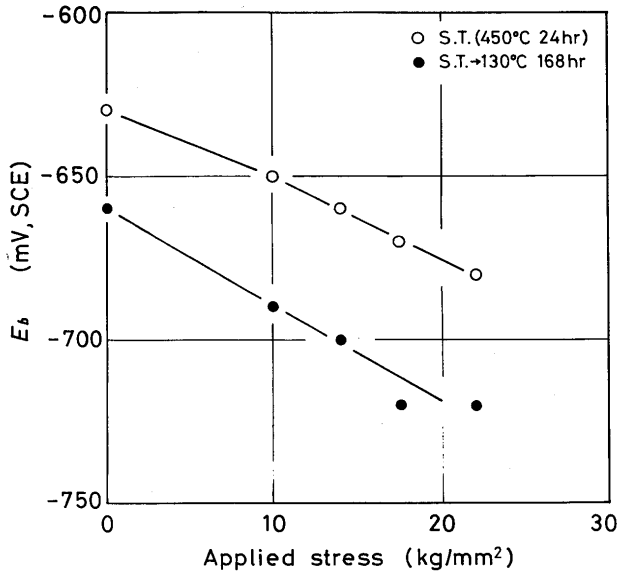

Fig. 3 Effect of applied tensile stress on breakdown potential (E_b) of 5083 aluminum alloy

concentration where the protection of surface film is weakened. E_b is considered to be the break down potential of films at grain boundary because the E_b of aged specimens with almost continuous β-phase precipitation at grain boundaries are always lower than those of as received and solution treated ones.

3.2 SCC tests

Figure 4 indicates the stress-strain curves of aged specimens strained in SCC test solution under various applied anodic potentials. Elongation and UTS reduced under anodic potentials. At −800 mV, elongation is only one half of that in an air atmosphere, and UTS is about 25% reduced. Further applied potential lowered elongation and UTS, however, the anodic potential dependence is slight in the rage of −750 ~ −640 mV. After reaching the maximum stress, the stress decreased gradually, showing serration-like curves with repeative drastic decrease and slow increase of stress. The drastic decrease of stress seems to correspond to the rapid propagation of SCC. The drastic decrease of stress is also observed in an air atmosphere, however, in the test in SCC solution, with the increase of potentials, the repetition of stress variation becomes frequent and the curve exhibits large decrement of stress from maximum stress to final fracture.

The relations between anodic potentials and mechanical properties (UTS and elongation) are shown in **Fig. 5** for specimens with different heat treatments. Similar tendency is obtained for elongation and strength against potentials. In aged specimens, the remarkable decrease of strength appears at −800 mV, but the reduction of elongation becomes remarkable at lower potentials (−860 mV ~ −800 mV). In the rage of −680 ~ −600 mV, all specimens represent constant values of mechanical properties irrespective to potentials. As the anodic dissolution current increases with the potential, the over potentials beyond −680 mV may accelerate only general corrosion. The reduction of elongation and UTS is due to the decrease of crosssection of material caused by the initiation and propagation of SCC during tensile test under constant strain rate. The decrement is strictly coincided with the SCC susceptibility[15), 17)]. In the range of −680 ~ −600 mV, where the mechanical properties are almost independent of potential (Fig. 5), SCC susceptibility of each specimens are clearly clasified; the materials become

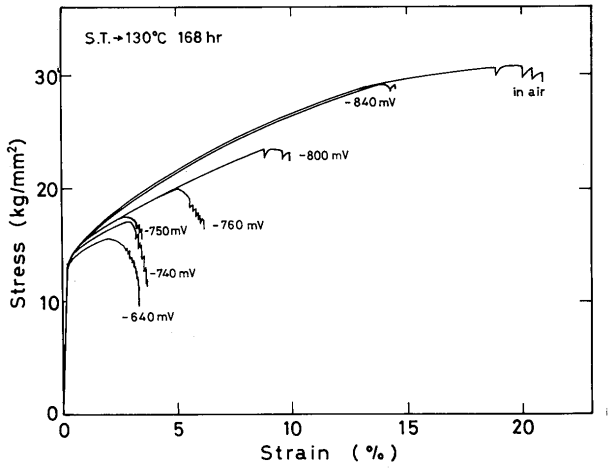

Fig. 4 Stress-strain curves of aged specimen in SCC test solution under various anodic potentials

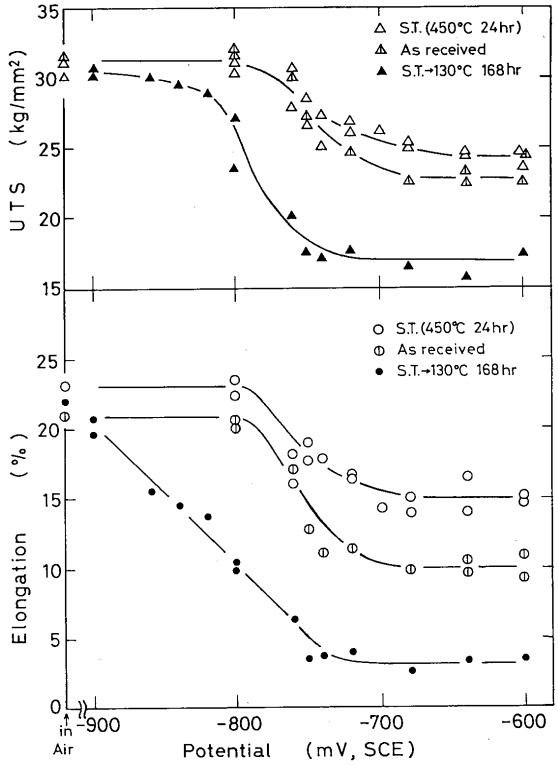

Fig. 5 Results of slow strain rate tensile test in SCC test solution under various anodic polarization potentials

sensitive to SCC in this order: solution treated, as received, and aged. The order corresponds to the amount of β-phase grain boundary precipitates[18].

As already indicated in Fig. 2, E_b of solution treated materials were −660 mV (polarization rate: 10 mV/5 min) under no load. Beyond the potential, surface films shifted from stable state to unstable state. By regarding the relations between E_b and stress have liniarity, extrapolation of the lines to the tensile strength of the alloy (about 30 kg/mm^2) gives the potentials of −700 mV and 750 mV for solution treated and aged materials respectively. SCC is observed at lower potentials (−760 mV for solution treated and less than −860 mV for aged materials) than above mentioned extraporated breakdown potentials. Taking into account that the local surface film breakdown is necessary for the initiation of SCC, the surface film becomes unstable and is broken at lower potentials under the constant strain rate *i.e.*, continuous straining than under the static load.

3.3 Fractographic observations

All materials irrespective to the heat treatment, showed ductile fracture in air atmosphere showing dimple patterns. **Figure 6** is an example of the aged material tested in air. SCC fractographs at several anodic potentials by constant strain rate test for each specimen are shown in **Fig. 7**. The top end of each photograph is the outer side of tensile test specimen. At −800 mV, solution treated material exhibiting same elongation as in air still shows dimple patterns similar to the fracture in air; but at −760 mV where elongation slightly reduced, facet pits are observed. The area ratio of pits to ductile fracture surface increased with the rise of potential. The fracture surface of as received material at −800 mV were dimple patterns almost similar to those in solution treated; at −760 mV, small facet pits were detected on relatively flat fracture surface. The aged materials at −840 mV, where the reduction of elongation initiated, exhibited partially the very

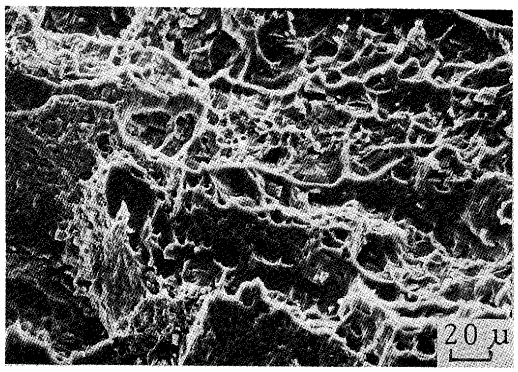

Fig. 6 Fractograph of aged specimen failed in air

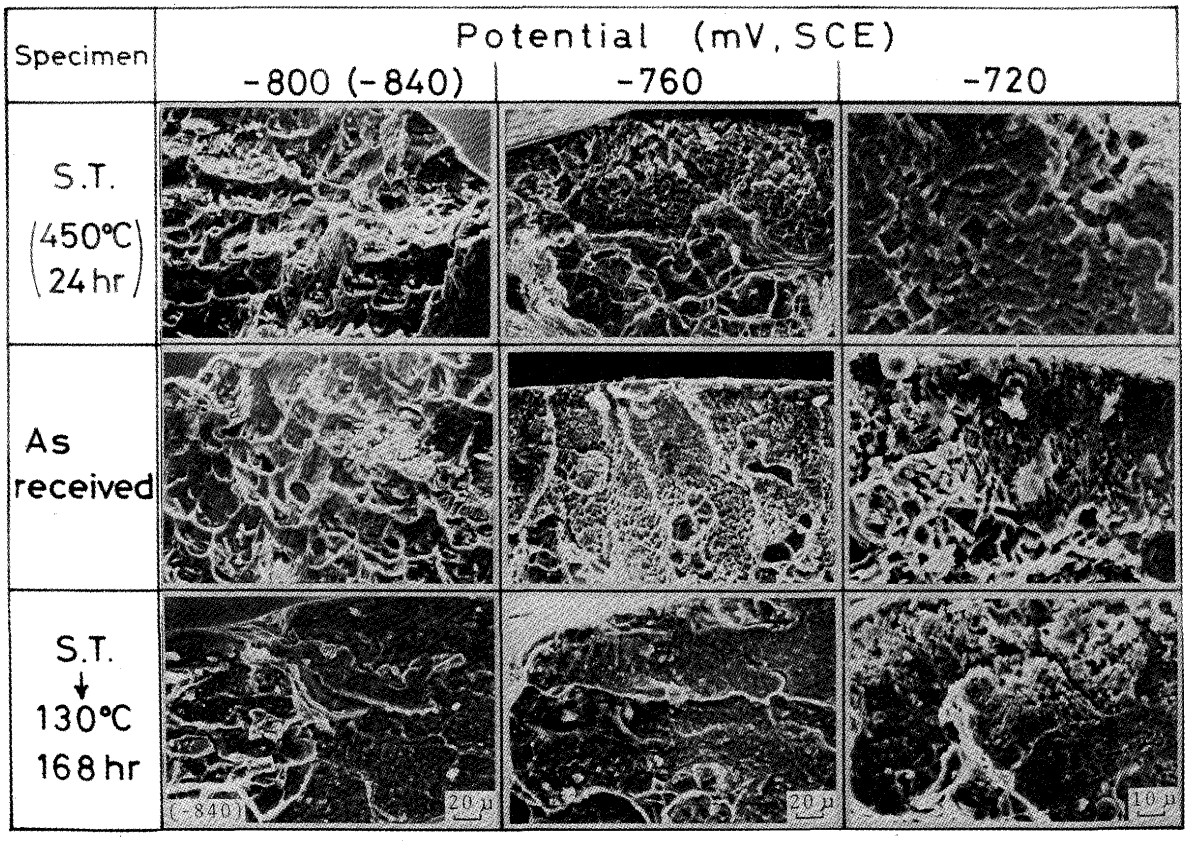

Fig. 7 Fractographs of SCC test specimens under various anodic polarization potentials

small amount of flat plane at outer side, but dimple fracture was predominant especially in the interior. The flat plane proceeded from outer surface to inside and the dimple patterned area reduced with the rise in applied potential. As the crosssectional observation confirmed the intergranular fracture, the flat plane demonstrates the grain boundary plane elongated along rolling direction. At −720 mV, outer area shows many facet pits and the rise in potential extended the pit area indicating severe corrosion. But the flat area still existed at interior of specimen (near the final fractured area). At −760 mV, all materials exhibited the reduction of elongation by SCC, facet pits are found at only the outer side and dimple pattern was dominant in solution treated specimens; as received specimen showed flat surface with small pits at outer side; aged specimen still presented flat fracture surface.

The pit area increased with the rise of potential in all materials, but the degree of increase was high in solution treated materials and low in aged materials. At −680 mV, fracture surface of solution treated materials were covered with facet pits of relatively large size than those formed at lower potentials. Aged materials were also covered with facet pits but the size and the irregurarity were small. In aged materials, facet pits were dominant only at outer area but the flat plane was observed at near the final fractured area. Therefore, the facet pits become dominant with the increase of anodic current density by the rise in applied potential; and the pits are dominant in low SCC susceptibility material, and also at the outer side that means they dominantly appear on the plane which has been exposed in corrosive solution for a long time. On the contrary, facet pits are not formed easily in materials with high SCC susceptibility (aged), which showed flat fracture surface in the neighborhood of final fractured area. Thus the pits in aged materials are resulted from the long time immersion in corrosive solution under applied anodic potentials on flat plane that was formed by the propagation of stress corrosion cracks.

Since the facet pits are easily formed by constant potential dissolution tests under no load[19),20)], there is no relations between the propagation of SCC and the existence of facet pits. Thus the pits are neither formed by the propagation of SCC cracks nor the evidence of SCC. From the fractured surface morphology, it is concluded that the materials with many facet pits have low SCC susceptibility and the materials with flat surface are highly sensitive to SCC.

3.4 Instabilization of surface film during potentiostatic holding

The SCC test results shown in Fig. 5 demonstrate that the reduction of elongation occured at lower (base) potentials than E_b in Fig. 3. The holding time at constant potential affects the unstabilization of surface film[16)]. Then, the effect of tensile stress on anodic current during potentiostatic holding at −700 mV was investigated (**Fig. 8**). The anodic current-time curves of solution treated were unaffected by the applied tensile stress of 14 kg/mm^2. The current began to increase within shorter time under the stress of 18 ~ 22 kg/mm^2 meaning the activation (instabilization) of surface film yielded easily under high stress levels. In aged materials, the time required to begin an increase of current was shorter than that of solution treated under the same testing conditions, which confirmed the surface film instability of aged materials. The mark x indicates the fracture of the specimen. The time that the current increase starts (T_b) is measured from the current-time curves at −700 mV (Fig. 8). The results are ploted as a function of applied stress (**Fig. 9**). T_b of aged materials are shorter than those of solution treated under all applied stresses. In solution treated materials, T_b significantly shifted to short time when the stress ex-

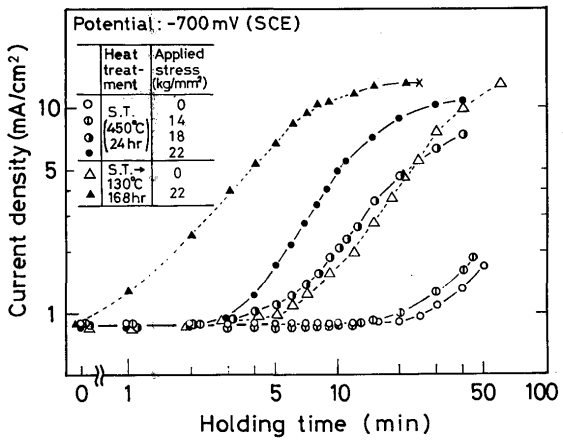

Fig. 8 Changes of current density during holding at −700 mV (SCE)

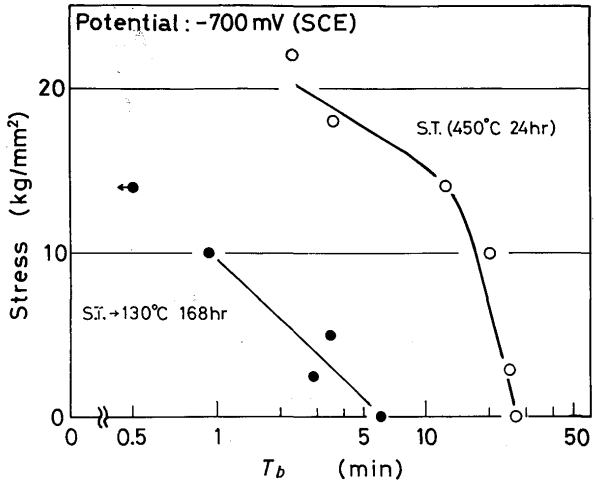

Fig. 9 Effect of applied tensile stress on time to breakdown (T_b) of surface films in SCC test solution

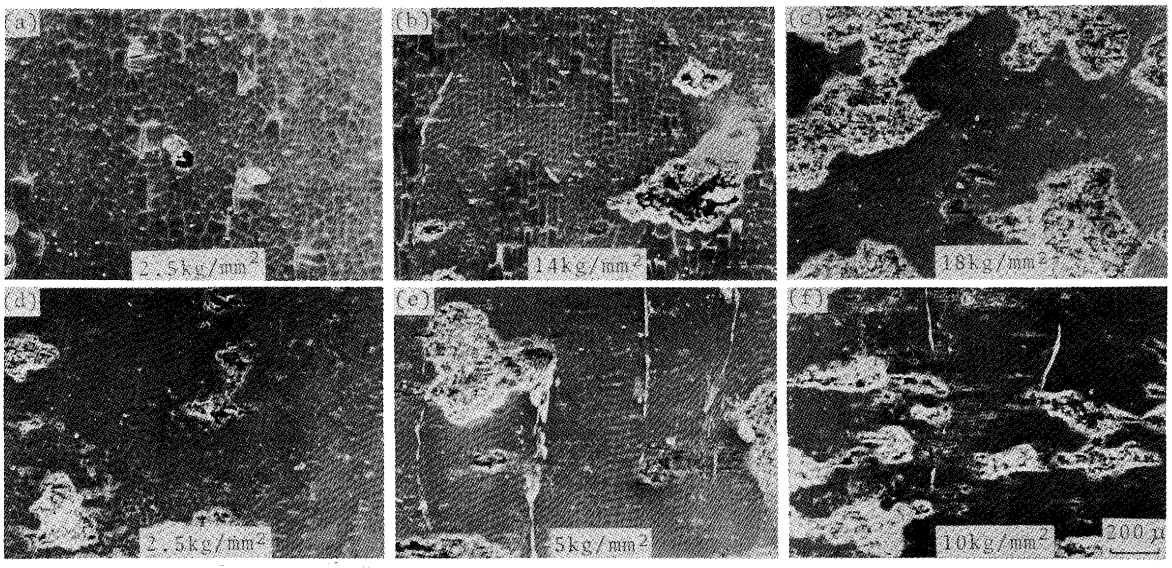

Fig. 10 Surface pits of 5083 aluminum alloy formed at −700mV (SCE) under various applied tensile stresses, (a) ~ (c): solution treated (450°C, 24 hr), (d) ~ (f): solution treated (450°C, 24 hr) and aged at 130°C for 168hr

ceeded the proof stress (about 14 kg/mm^2). It is clear that the surface film becomes unstable in short times under tensile stress.

Figure 10 is the surface of the specimen tested at −700 mV for 45 min under various applied stress. At 2.5 kg/mm^2, pits are scarcely observed in solution treated, however, large and many pits are found in aged materials. The pit area incrased with the increase of applied stress. In aged materials, small pits are linked with each other along normal direction to tensile axis (tensile axis is top and bottom direction of the figure). Since SCC occured remarkably at −700 mV, the linking of pit led the stress corrosion cracks under tensile stress. In aged materials some pit areas elongated along normal direction to applied stress, but on the whole, the directionality is slight.

The effect of holding potential and constant straining on the time required for instabilization of surface film (T_b) was investigated. **Figure 11** shows T_b which was determined from the current-time curves of aged and solution treated materials by holding at various potentials. The results indicated by solid circles are obtained by constant straining of 0.05 mm/min, and the ones indicated by open circles are obtained under no load. The rightward arrows indicate that the increment of current was not observed by holding more than 80 min under no load. The marks x demonstrate that the remarkable increase in current was not identified until the fracture of constant strain rate tensile specimen.

The following results are clear from Fig. 11, first: the aged materials with continuous β-phase grain boundary precipitates have shorter T_b than solution treated materials at all potentials; second: the linear relationships are

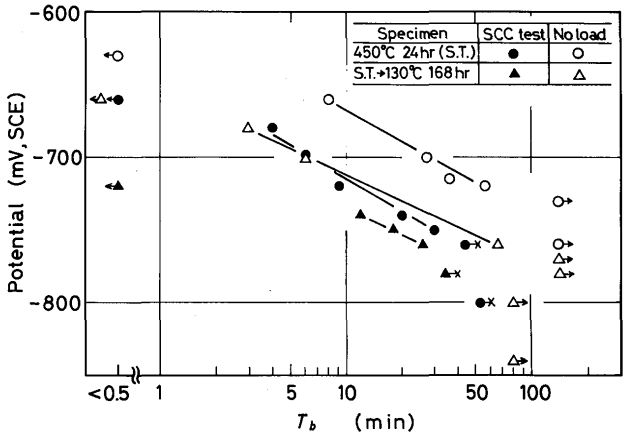

Fig. 11 Effect of continuous strain on time to breakdown (T_b) of surface films of 5083 aluminum alloy.

present between holding potential and *log* T_b in certain potential ranges; third: the applied continuous strain accelerates the instabilization of surface films and shifts T_b to shorter time; forth: the highest potential at which T_b is not identified within 1 hr test under no load ($E^0{}_{Tb}$) is −730 mV for solution treated and −770 mV for aged materials respectively.

4. Discussions

From the SCC fracture surface observation, the facet pits are found to appear remarkably in materials with low SCC susceptibility and the flat surface is dominant in the aged specimen with continuous β-phase precipitation at grain boundaries. The rise in applied potential increased anodic current and resulted remarkable pits, but elongation during SCC test is not varied in the range of −720 ~

−600 mV. Higashi *et al.*[21] mentioned that β-phase is retained on flat grain boundary fracture surface in Al-8%Mg alloy, and they suggested dominant mechanical fracture rather than corrosion. In the present experiment, SCC test in the potential range of −860 ~ −800 mV showed reduction of elongation and flat fracture surface, and T_b is not observed. Accordingly, the mechanical factors seems to act effectively rather than corrosive reaction in that potential range. The SCC mechanism of 5083 aluminum alloy appears to depend on the holding potential; the mechanical fracture is dominant in the neiborhood of the SCC initiating potential and the corrosion reaction is remarkable above the potentials where T_b appears during SCC test.

Figure 12 shows the facet pits formed after polarization at −720 mV under no load. The facet pits are also observed in the other anodic polarization experiments under no load[19), 20)] which indicates that the formation of facet pit is not always attributable to the mechanochemical corrosion reaction under the stress. As the applied stress enhanced the formation and growth of pits, it also appears to be true that the pit initiation is difficult under mere immersion without applied potential and/or load[21)]. As mentioned above, the materials with difficulty to form facet pits are more sensitive to SCC than the ones that form pits easily. Accordingly, the facet pit in SCC fracture surface is not the characteristic feature of SCC of 5083 aluminum alloy.

The relations between holding potential and log T_b were linear (Fig. 8). Similar linearities were also obtained by Sugimoto *el al.*[22)] on aluminum. When the continuous strain is applied, the repair rate of broken film could not keep up with the breakdown rate of surface films under continuous straining, because the continuous strain resulted the continuous breakdown of surface films. As a result, the film looses the protectivity easily, thus the T_b shifted to shorter time. T_b of solution treated material under applied stress of 10 and 22 kg/mm^2 at −700 mV were 20 and 2.2 min respectively (Fig. 9). On the other hand,

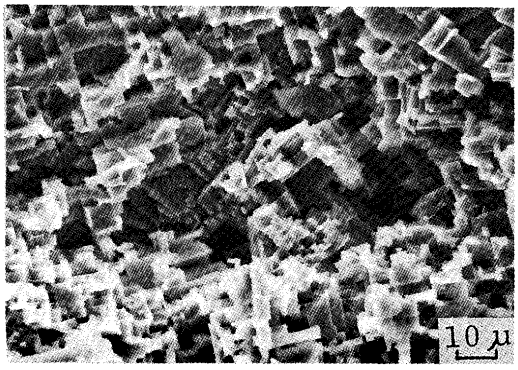

Fig. 12 Pits formed in as received specimen at −720mV (SCE) under no load

T_b under continuous straining at −700 mV was 6 min (Fig. 11), which is longer than that obtained under the stress of 22 kg/mm^2; it seems that the static load is more effective than continuous straining for the instabilization of surface films, however, in continuous strain rate test, the applied stress was less than 10 kg/mm^2 at 3 min after the start of straining. Under this static stress level, T_b is more than 20 min (Fig. 9). Therefore, the continuous straining is more effective than static stress on the reduction of T_b. Since the reduction of elongation by SCC is found at the base potential range (−760 mV for solution treated and −770 ~ −800 mV for aged materials respectively) at which the T_b is not found until the fracture of SCC test specimen, the mechanical fracture seems to be more effective on the initiation and the propagation of SCC than electrochemicaldissolution reaction in these potential ranges.

SCC of 5083 aluminum alloy initiated at lower potentials than the breakdown potential of surface film (E_b) under no load. Accordingly, the SCC initiation potential could not be estimated from the E_b obtained by the rise in anodic current of polarization curves. The fact that the SCC initiation potential is lower than E_b is very similar to that the SCC potentials of stainless steels existed at slightly lower potentials than the pitting potentials[23), 24)].

SCC ocuures at the potential where the surface film does not change from stable to unstable state by holding for certain time under anodic polarization. Therefore, the occurrence of SCC cannot be estimated from the absence or presence of T_b by holding at constnat potential under no load. **Figure 13** shows the anodic polarization curves of solution treated and aged materials. To obtain the protection potential, polarization direction is returned to base direction at the current density of 20 mA/cm^2. The polarization rate was 20 mV/30 sec up to −900 mV, and 10 mV/min above −900 mV. The figure shows the polariza-

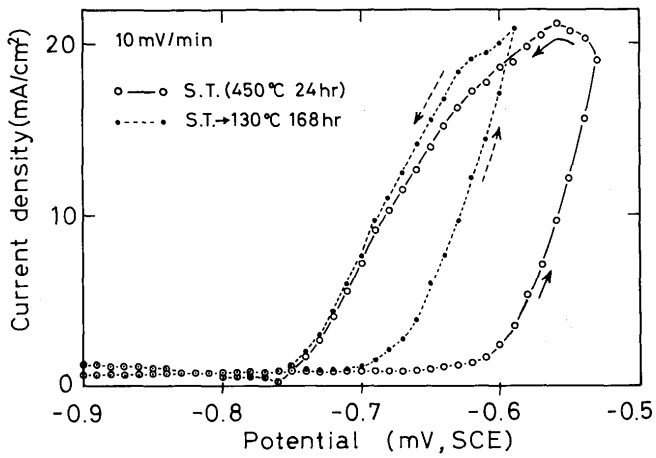

Fig. 13 Anodic polarization curves of solution treated and aged specimens for the measurement of protection potentials

tion curves above −900 mV, E_b of aged material is lower than that of solution treated, however, the protection potentials are the same (−750 ~ −760 mV) irrespective to the microstructure of specimens. The protection potentials may coincide with the cease of the growth of pit formed in grain interior, it is clear that the protection potential has no corelations with the SCC initiation potentials. However, above the protection potentials, all specimens showed remarkable SCC. The following discussions deal with the potentials that does not offer SCC.

The surface film breakdown potential (E_b) can be expressed by the following function from the present experiment.

$$E_b = f(\tau, \sigma, \epsilon, M, \ldots) \quad (1)$$

, where, τ : polarization rate,
σ : applied stress,
ϵ : continuous straining,
M : heat treatment of material (microstructure).

The other factor such as the activity of chloride ions in corrosive solution[25] has also considerable influence on SCC, but it was constant in the present work. Under the constant polarization rate (τ), the relation between applied stress (σ) and E_b are expressed as follows from Fig. 3.

$$E_b = E_0 - \alpha\sigma \quad (2)$$

, where, E_0 : surface film breakdown potential under constant polarization rate and without applied stress,
α : stress dependent coefficient (positive constant).

As shown in Eq. (1), E_b is a function of τ, but assuming there is no change in α of Eq. (2) in some ranges of τ, the applied stress of 30 kg/mm^2 (about UTS of both aged and solution treated materials) will shift the E_b toward base directions about 70 mV (−700 mV, SCE) for solution treated and 90 mV (−750 mV, SCE) for aged materials respectively (Fig. 3). On the other hand, the highest potential where the surface film breakdown does not appear by holding at constant potential under no applied stress ($E^0{}_{Tb}$) were −730 mV and −770 mV for solution treated and aged materials respectively (Fig. 11). If the effect of applied stress on $E^0{}_{Tb}$ is the same on E_b, *i.e.*, α is a constant, the highest potential where the surface film breakdown does not appear under the applied stress of UTS ($E^U{}_{Tb}$) is expressed as follows,

$$E^U{}_{Tb} = E^0{}_{Tb} - \Delta E_U \quad (3)$$

, where, ΔE_U : change of E_b by applying UTS.

Thus, the highest potentials where the surface film breakdown potential does not appear by applying the stress of UTS (30 kg/mm^2), $E^U{}_{Tb}$, are derived from Eq. (3) as −800 mV and −860 mV for solution treated and aged materials respectively. In fact, the reduction of stress and elongation was not found in solution treated specimens at −800 mV. In aged materials, elongation slightly decreased at −860 mV, however, SCC does not occur completely at −900 mV. The difference between the experiment and the above calculation is only 40 mV. Therefore, the highest potential where SCC is not appear can be expressed approximately by $E^U{}_{Tb}$ in Eq. (3).

5. Conclusions

Continuous strain rate stress corrosion cracking test, anodic polarization tests under tensile stress and fractographic observations have been performed on 5083 aluminum alloy in NaCl + H_2O_2 solution. The obtained results are summarized as follows.

(1) The breakdown potential of surface film (E_b) is found to depend on polarization rate, microstructure of alloy, applied stress, and continuous straining. The slow anodic polarization rate, increase of β-phase precipitates and applied stress shifted E_b to base direction.
(2) The time to the initiation of increase of anodic current by holding at constant anodic potentials, T_b also shifted to base directions by low temperature aging, applied stress and straining.
(3) The potential where the SCC does not occur can be expressed approximately by using the highest potential where the surface film does not shift to unstable state ($E^0{}_{Tb}$) and the change of E_b by applying the stress of UTS (ΔE_U). In other words, the highest stress where SCC does not occur can be estimated from the stress dependence of E_b and $E^0{}_{Tb}$.
(4) The facet pits in SCC fracture surface is apt to appear in the materials with low SCC susceptibility. The facet pits are neither the characteristic feature of SCC of 5083 aluminum alloy nor the evidence of the propagation of stress corrosion cracks.
(5) The facet pits on surface become remarkable with the increase of applied stress under constant potential for certain time.

Acknowledgment

The expence of this investigation was supported by the Science Research Budget of Ministry of Education (Encouradgement Research A). The authers would like to thank Mr. S. Tsutsumino for experimental works. Thanks are also to Kawasaki Heavy Insustries Co., Ltd. for presentation of materials.

References

1) E.C.W. Perryman and G.B. Brook: J. Inst. Metals, 79 (1951), 19.
2) A. Eikum and G. Thomas: Acta Met., **12** (1964), 537.
3) W.W. Binger, E.H. Hollingsworth and D.O. Sprowls: *Aluminum*, **Vol. 1**, ASM (ed. by K.R. Horn), (1967), 209.
4) S. Muromachi, T. Yamada and T. Mae: J. Japan Inst. Light Metals, **25** (1975), 123 (in Japanese).
5) S. Ohsaki, Y. Kojima and T. Takahashi: J. Japan Inst. Light Metals, **25** (1975), 173 (in Japanese).
6) E.C.W. Perryman and S.E. Hadden: J. Inst. Metals, 77 (1950), 207.
7) E.H. Dix Jr., W.A. Anderson and M.B. Shumaker: Corrosion, **15** (1959), 55t.
8) H.L. Craig, Jr., and H.B. Romans: *Stress Corrosion Testing*, ASTM, STP **425** (1967), 51.
9) S. Ohsaki, Y. Kojima and T. Takahashi: J. Japan Inst. Light Metals, **25** (1975), 18 (in Japanese).
10) S. Hori, T. Takemoto and K. Morimoto: J. Japan Inst. Light Metals, **27** (1977), 33 (in Japanese).
11) T. Ohnishi, Y. Nakatani and H. Sakamoto: J. Japan Inst. Light Metals, **26**, (1976), 8 (in Japanese).
12) K. Goto, Y. Shimizu and G. Ito: J. Japan Inst. Light Metals, **27** (1977), 332 (in Japanese).
13) D.O. Sprowls and R.H. Brown: *Proceedings of Conference on Fundamental Aspects of Stress Corrosion Cracking*, (1967), Ohio State Univ., 466.
14) N. Ohotani, Y. Fujishima, H. Sato, K. Ito: J. Japan Inst. Metals, **37** (1973), 295 (in Japanese).
15) S. Ohsaki, Y. Kojima and T. Takahashi: J. Japan Inst. Light Metals, **27** (1977), 138 (in Japanese).
16) T. Izaki and K. Arai: J. Japan Inst. Metals, **31** (1967), 1023 (in Japanese).
17) J. H. Payer, W.E. Berry and W.K. Boyd: Stress Corrosion Cracking—The Slow Strain-Rate Techniques, ASTM-STP **665**, (1979), 61.
18) T. Takemoto and I. Okamoto: J. Light Metal Welding & Construction, **21** (1983), 206 (in Japanese).
19) K. Tohma, Y. Sugai and Y. Takeuchi: J. Japan Inst. Light Metals, **31**, (1981), 157 (in Japanese).
20) Y. Takatani and T. Yokoyama: Denki Kagaku, **46** (1978), 608., **49** (1981), 50 (in Japanese).
21) K. Higashi, T. Ohnishi, Y. Nakatani and K. Okabayashi: J. Japan Inst. Light Metals, **30** (1980), 560 (in Japanese).
22) K. Sugimoto: Bohshokugijutsu, **20** (1971), 443 (in Japanese).
23) T. Shibata and T. Takeyama: J. Japan Inst. Metals, **38** (1974), 124 (in Japanese).
24) B.E. Wilde: J. Electrochem. Soc., **118** (1971), 1717.
25) H. Böhni, H.H. Uhlig: J Electrochem. Soc., **116** (1969), 906.